PHYSICS

Qubit analog with polariton superfluid in an annular trap

Joris Barrat[1,2,3], Andreas F. Tzortzakakis[4,5], Meng Niu[1,2,3], Xiaoqing Zhou[2,3], Giannis G. Paschos[2,3], David Petrosyan[4,6], Pavlos G. Savvidis[2,3,4]*

We report on the experimental realization and characterization of a qubit analog with semiconductor exciton-polaritons. In our system, a polaritonic condensate is confined by a spatially patterned pump laser in an annular trap that supports energy-degenerate vortex states of the polariton superfluid. Using temporal interference measurements, we observe coherent oscillations between a pair of counter-circulating vortex states coupled by elastic scattering of polaritons off the laser-imprinted potential. The qubit basis states correspond to the symmetric and antisymmetric superpositions of the two vortex states. By engineering the potential, we tune the coupling and coherent oscillations between the two circulating current states, control the energies of the qubit basis states, and initialize the qubit in the desired state. The dynamics of the system is accurately reproduced by our theoretical two-state model, and we discuss potential avenues to implement quantum gates and algorithms with polaritonic qubits analogous to quantum computation with standard qubits.

INTRODUCTION

Exciton-polaritons are hybrid light-matter bosonic quasiparticles resulting from the strong coupling of semiconductor excitons and microcavity photons (*1*, *2*). The polaritons combine an extremely small effective mass, inherited from their photonic component, with strong nonlinearities, inherited from their excitonic component. As a result, polaritons can exhibit macroscopic spatial coherence and form out-of-equilibrium condensates exhibiting superfluid behavior at elevated temperatures when pumped above threshold (*3*, *4*). Furthermore, the dissipative nature of polaritonic condensates, primarily stemming from their photonic component, enables interferometric measurements of condensate luminescence and extraction of the macroscopic wave function while still maintaining long coherence times. Given their unique properties, exciton-polaritons represent an attractive platform for exploring quantum collective phenomena and hold promise for a variety of applications, including low-threshold lasing (*5*, *6*), efficient energy transfer (*7*–*9*), and simulation of many-body systems (*10*–*12*).

A promising recent theoretical proposal for quantum computing uses split-ring polariton-condensate qubits involving quantized circular currents (*13*, *14*). This system relies on the formation of vortices in superfluids arising from the quantization of circulation, where the phase accumulation around a supercurrent loop can only take discrete values. Closely related physics governs the principles of operation of superconducting flux or phase qubits involving superconducting loops interrupted by Josephson junctions (*15*–*18*).

Following their initial observation in planar unconfined geometries (*19*–*23*), quantized vortices and persistent circulating currents of exciton-polariton superfluids have been observed and studied in various ring-shaped geometries, including optically induced traps (*24*–*28*) or confinement in etched micropillars (*29*, *30*). Previous efforts to generate polariton condensates with nonzero orbital angular momentum (OAM) used phase-shaped external laser beams (*31*–*34*) or optically generated nearly defect-free potentials (*35*–*38*). These techniques have successfully overcome the limitations imposed by intrinsic potential disorder which often leads to phase locking and the formation of standing waves manifested by petal-shaped patterns pinned by the defects (*39*–*42*). Moreover, slightly detuned Laguerre-Gaussian beams with nonzero OAM have been used to stir the trapping potential and control the vorticity of the superfluid (*43*). So far, however, none of these approaches have achieved controllable superpositions of vortex states.

Here, we show that, under appropriate conditions, optically trapped nonequilibrium polariton condensates can populate two well-characterized vortex states corresponding to the clockwise and counterclockwise circulating currents. We demonstrate coherent coupling between these energy-degenerate states, due to the partial reflection of the circulating superfluid from a weakly disordered laser potential or an external control laser beam, while simultaneously maintaining long coherence times.

We can control the coupling between the vortex states and thereby the energy splitting between the two eigenmodes of the system corresponding to the symmetric and antisymmetric superposition of the vortex states. Inspired by the theoretical proposal to realize qubit analogs and quantum computing with two-mode Bose-Einstein condensates (*44*), we formally identify the two polaritonic eigenmodes with the basis states of a qubit. Supplemented with controllable coupling between individual polaritonic qubits, such systems hold great potential for simulating a subset of quantum algorithms that do not rely on entanglement (*45*–*48*).

RESULTS

Polaritonic qubit analog

Our system is illustrated in Fig. 1. A spatially patterned pump laser creates a Mexican hat–shaped trapping potential of appropriate size for the polaritons (Fig. 1B). When pumped slightly above the

[1]Department of Physics, Fudan University, Shanghai 200433, China. [2]Key Laboratory for Quantum Materials of Zhejiang Province, Physics Department, Westlake University, 18 Shilongshan Rd, Hangzhou 310024, Zhejiang, China. [3]Institute of Natural Sciences, WIAS, 18 Shilongshan Road, Hangzhou, Zhejiang Province 310024, China. [4]Institute of Electronic Structure and Laser, FORTH, 70013 Heraklion, Crete, Greece. [5]Department of Physics, National and Kapodistrian University of Athens, 15784 Athens, Greece. [6]A. Alikhanyan National Science Laboratory (YerPhI), 0036 Yerevan, Armenia.
*Corresponding author. Email: p.savvidis@westlake.edu.cn

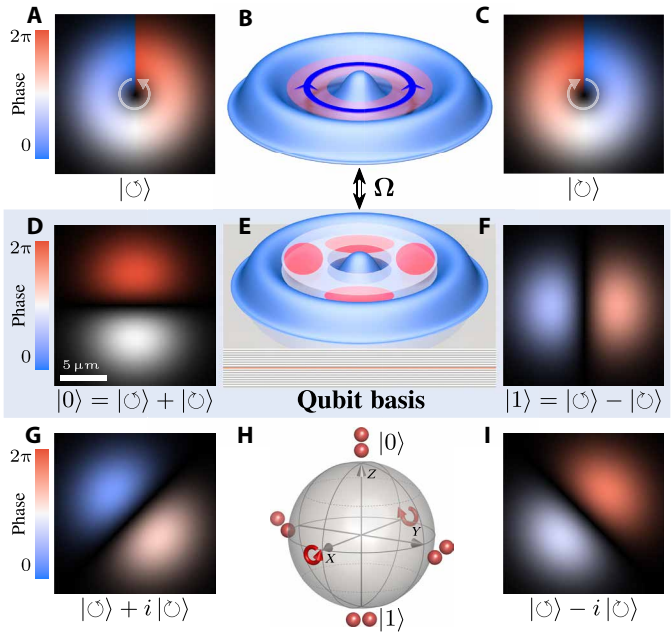

Fig. 1. Schematics of the polaritonic qubit analog. A pump laser creates a Mexican hat–shaped potential for the polaritonic condensate (**B**). The potential supports two energy-degenerate counter-circulating polariton modes $|\circlearrowleft\rangle$, $|\circlearrowright\rangle$ (**A** and **C**), which are coupled with rate Ω by small defects or ellipticity of the trapping potential. The resulting superpositions $(|\circlearrowleft\rangle \pm |\circlearrowright\rangle)/\sqrt{2}$ of the two vortex modes form vertically and horizontally oriented two-lobe eigenmodes (**D** and **F**) that represent the qubit basis states $|0,1\rangle$ energy split by $\mp\Omega$ (**E**). Another pair of states $e^{\pm i\pi/4}(|\circlearrowleft\rangle \mp i|\circlearrowright\rangle)/\sqrt{2}$ with diagonally oriented lobes (**G** and **I**) represents the third axis of the Bloch sphere (**H**) for the continuum of states of the system. In (A), (C), (D), (F), (G), and (I), the shading is proportional to the amplitude of the polaritonic condensate, and the color encodes its phase varying from 0 to 2π.

condensation threshold, the polaritons condense into two energy-degenerate counter-circulating vortex states $|\circlearrowleft\rangle$ and $|\circlearrowright\rangle$ whose wave functions can be well approximated by the Laguerre-Gaussian modes with orbital angular momenta $l = \pm 1$

$$\psi_{\circlearrowleft,\circlearrowright}(\boldsymbol{r}) = C\ \rho\ e^{-\frac{1}{2}(\rho/\rho_c)^2}\ e^{\pm i\theta} \tag{1}$$

where we use cylindrical coordinates $\boldsymbol{r} \equiv (\rho, \theta, h = 0)$, ρ_c is the mean radius of the condensate, and C is a normalization constant.

Small defects and weak ellipticity of the confining potential result in backscattering of the polariton current and thereby coherent coupling between the states $|\circlearrowleft\rangle$ and $|\circlearrowright\rangle$ with rate Ω. We may formally associate our system with a spin-$^1/_2$ system via mapping $|\circlearrowleft, \circlearrowright\rangle \rightarrow |\uparrow, \downarrow\rangle_x$, $e^{\pm i\pi/4}\frac{|\circlearrowleft\rangle \mp i|\circlearrowright\rangle}{\sqrt{2}} \rightarrow |\uparrow, \downarrow\rangle_y$, and $\frac{|\circlearrowleft\rangle \pm |\circlearrowright\rangle}{\sqrt{2}} \rightarrow |\uparrow, \downarrow\rangle_z$ and write the Hamiltonian for the two coupled vortex states as ($\hbar = 1$)

$$H = -\Omega\,|\circlearrowleft\rangle\langle\circlearrowright| + \text{H.c} = -\Omega\sigma_z \tag{2}$$

where $\sigma_z = |\uparrow\rangle_z\langle\uparrow| - |\downarrow\rangle_z\langle\downarrow|$ is the Pauli spin operator, while Ω plays the role of the effective longitudinal magnetic field (along the z direction) that results in energy splitting $\mp\Omega$ between the states $|\uparrow\rangle_z$ and $|\downarrow\rangle_z$ shown in Fig. 1E. We can thus assign to the lower and higher energy states the qubit basis states $|0,1\rangle \equiv |\uparrow, \downarrow\rangle_z$. The continuum of states of the system is conventionally represented by the Bloch sphere, see Fig. 1H.

The spatial wave functions of the states $|\uparrow, \downarrow\rangle_{x,y,z}$ are shown in Fig. 1, A, C, G, I, D, and F, respectively. We observe that the vortex states $|\uparrow, \downarrow\rangle_x = |\circlearrowleft, \circlearrowright\rangle$ have azimuthally uniform amplitude and phase increasing from 0 to 2π in counterclockwise and clockwise directions, whereas the vortex superposition states $|\uparrow, \downarrow\rangle_y$ and $|\uparrow, \downarrow\rangle_z$ have two lobes with diagonal and vertical/horizontal orientations with the phase difference π between the lobes. With the convention that the potential energy bump or minor axis of the ellipse of the confining potential is oriented horizontally, the eigenmode $|\uparrow\rangle_z$ with the vertically oriented lobes has lower energy, and the eigenmode $|\downarrow\rangle_z$ with horizontally oriented lobes has higher energy.

Experimental setup

The experiments are carried out at a cryogenic temperature of 11 K in a semiconductor microcavity consisting of four sets of three GaAs quantum wells placed at an antinode of a high finesse cavity formed by AlGaAs/AlAs Bragg mirrors. The sample is excited by a continuous wave laser, pumping a reservoir of excitons, some of which relax to form polaritons. The excitonic reservoir also induces a repulsive potential for the polaritons via interaction with their excitonic component. Details of the experimental setup are given in Supplementary Materials S1.

The pump laser is spatially patterned using a spatial light modulator (SLM) to imprint a Mexican hat–shaped potential with a radius of ~9 μm to confine the polaritons. In such a small trap, just above the condensation threshold $P \approx 1.2\ P_{\text{th}}$ for the polaritons, we observe only a narrow energy mode, while for stronger pumping $P > 1.5\ P_{\text{th}}$, the reservoir of excitons can populate many discreet polariton modes. This is verified by measuring the angle-integrated photoluminescence intensity and extracting the normalized power density of spectrometer charge-coupled device (CCD; energy resolution per pixel is 45 μeV), as shown in Fig. 2A.

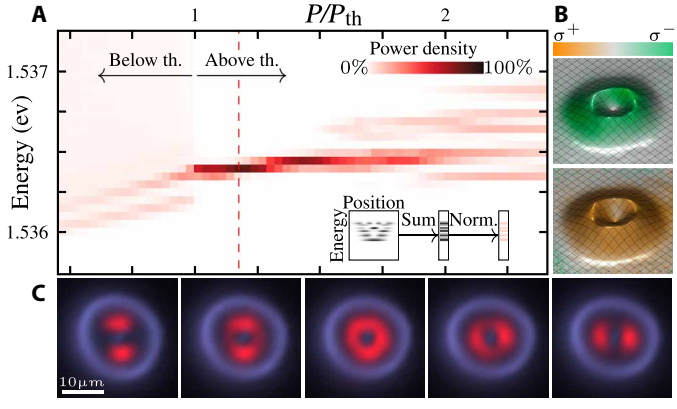

Fig. 2. Polariton condensate in an annular trap. (**A**) Integrated photoluminescence spectrum of polaritons versus the pumping strength P, with inset illustrating the schematics of the measurement. Slightly above the condensation threshold $P = 1.2P_{\text{th}}$ (vertical dashed line), the polaritons condense to the vortex states with orbital angular momenta $l = \pm 1$ having the same energy. (**B**) Polariton condensate intensity (profile height) and spatially resolved degree of circular polarization (color) for σ^- (top) or σ^+ (bottom) polarized pump laser. The circularly polarized pump generates polariton condensate with the same spatially uniform polarization. (**C**) Polariton condensate photoluminescence (red) for increasing (from left to right) ratios of the horizontal and vertical axes of the elliptic profile of the pump laser (blue).

In what follows, we consider the single-mode regime of weak pumping $P \approx 1.2\ P_{\mathrm{th}}$. Inside the trap, the bosonic polaritons form an annular condensate with a mean radius $\rho_c \simeq 4$ μm, spatially separated from the reservoir excitons injected by the pump, see Fig. 2C. The trapping also suppresses the spin-obit coupling of the polaritons (*49*–*55*), and we observe a high degree of polarization of the condensate (*56*) strongly correlated with the polarization σ^+ or σ^- of the pumping laser, see Fig. 2B.

A nearly perfectly circular trapping potential imposed by the pump laser supports a ring-shaped polariton condensate consisting of two coupled counter-rotating superfluid vortex modes, as described above. When the pump laser profile is elliptic, we observe the double-lobe (standing-wave) structure oriented along the major axis of the ellipse, see Fig. 2C. We therefore engineer the spatial profile of the pump laser via precise control of the SLM to minimize the ellipticity of the trapping potential.

Dynamics of the system

The polariton condensate governed by Hamiltonian (*2*) undergoes Rabi-like oscillations between the two vortex states $|\circlearrowleft\rangle \equiv |\uparrow\rangle_x$ and $|\circlearrowright\rangle \equiv |\downarrow\rangle_x$ with frequency Ω (see Fig. 3), and the state of the system at any time t can be cast as

$$|\psi(t)\rangle = \cos\left(\Omega t + \phi_0\right)|\circlearrowleft\rangle + i\sin\left(\Omega t + \phi_0\right)|\circlearrowright\rangle \tag{3}$$

where ϕ_0 is some initial phase of the oscillations. This dynamics can be visualized on the Bloch sphere as a precession in the *xy* plane with the rate Ω.

To resolve experimentally the dynamics of the system, we perform interferometric measurements of the polariton photoluminescence. The light emanating from the poslaritonic condensate $\psi(\boldsymbol{r}, t)$ is split by a beamsplitter and sent into two arms of an interferometer. In one arm, the signal beam passes through a variable delay line to introduce time delay τ. In the other arm, the beam is expanded, and the field at position $\boldsymbol{r}_0 = (\rho_0, \theta_0)$ is taken as a reference with nearly uniform amplitude and phase front in the plane perpendicular to the propagation direction. The two beams are combined on a CCD camera with long exposure time T, resulting in interferometric image

$$\langle I(\boldsymbol{r}, \tau)\rangle \propto \frac{1}{T}\int_0^T |\psi(\boldsymbol{r}, t+\tau)e^{i\mathbf{k}_S\cdot r} + \psi\left(\boldsymbol{r}_0, t\right)e^{i\mathbf{k}_R\cdot r}|^2 \tag{4}$$

where $\boldsymbol{k}_{S,R}$ are the wave vectors of the signal and reference beams, and $\Delta\boldsymbol{k} \equiv \boldsymbol{k}_R - \boldsymbol{k}_S$ determines the spatial separation of the interference fringes.

In Fig. 3 (A and B), we show the experimentally obtained interferograms for $\rho_0 \simeq \rho_c$ and $\theta_0 \simeq \pi/4$ at different time delays τ and compare them with the theoretical model revealing excellent agreement. By performing Fourier analysis (*30*, *57*) of the images $\langle I(\boldsymbol{r}, \tau)\rangle$ (see Supplementary Materials S2 for details), we can retrieve the polariton wave function as

$$\mathcal{I}_{-\Delta k}(\boldsymbol{r}, \tau) = e^{-i\pi/4}\ \psi(\boldsymbol{r}, t=\tau) \quad \left(\phi_0 = \pi/4\right) \tag{5}$$

where $\mathcal{J}_{-\Delta k}$ is the corresponding Fourier component centered around $-\Delta\boldsymbol{k}$. The wave function oscillates between the $\psi_{\circlearrowleft}(\boldsymbol{r})$ and $\psi_{\circlearrowright}(\boldsymbol{r})$ vortex modes with period $\Delta\tau = \pi/\Omega$, see Fig. 3C. Using an additional weak control beam to introduce a potential barrier that reflects the polariton currents, we can thereby enhance the coupling between the two vortex states leading to oscillations with increased frequency Ω.

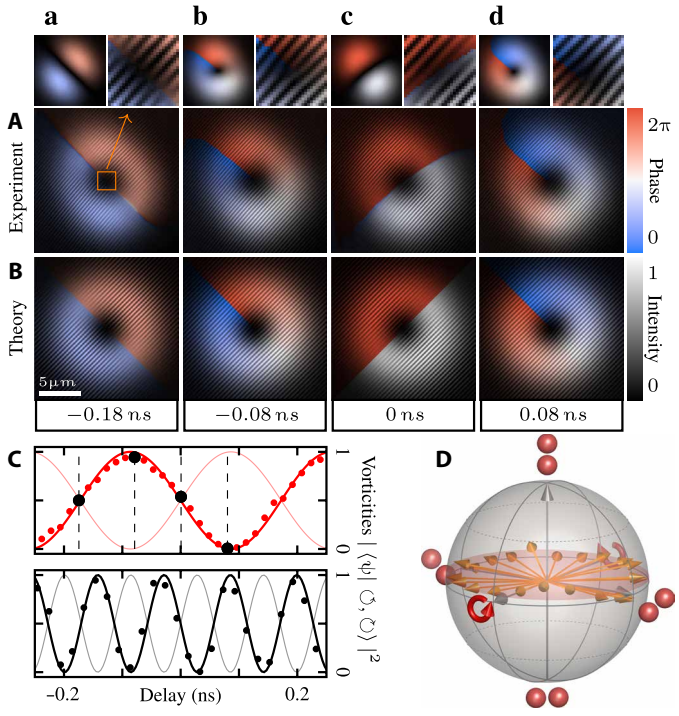

Fig. 3. Interferometric measurement of the system dynamics. Time-averaged spatial interferograms of the polaritonic condensate at four different delay times τ = −0.18, −0.08, 0, and 0.08 ns between the signal beam and the reference taken at $\rho_0 \simeq \rho_c$ and $\theta_0 \simeq \pi/4$, as obtained from the experimental measurements (**A**) and theoretical model (**B**). The condensate amplitude extracted from the interferometric images and the magnified view of the center of interferograms reveal the presence or absence of singularity (fork-shaped interference fringes) associated with the vortex states (a, b, c, and d). The polariton wave function ψ exhibits continuous oscillations with frequency Ω between the two vortex states $|\circlearrowleft\rangle$ and $|\circlearrowright\rangle$, quantified by vorticities $|\langle\psi|\circlearrowleft, \circlearrowright\rangle|^2$ (**C**). Introducing a potential barrier that enhances the scattering between the vortex states increases the oscillation frequency [bottom in (C)]. On the Bloch sphere, the dynamics of the system corresponds to precession in the *xy* plane slightly biased towards *z* direction (ground state $|0\rangle$) (**D**).

In Fig. 4, we illustrate in greater detail the influence of a tightly focused control beam on the dynamics of the system. A weak control beam creating a potential bump smaller than the intrinsic defects of the trap does not change noticeably the oscillation frequency between the two vortex states $|\circlearrowleft\rangle$ and $|\circlearrowright\rangle$. But increasing the control beam intensity and thereby the height of the potential barrier enhances the scattering of the polaritons between the counter-circulating vortex modes, which in turn leads to faster oscillations with decreasing amplitude. For very strong control beam, the condensate is pinned to a standing-wave (double-lobe) mode with a node at the control beam position.

In the spin language, the control beam at any position of the annular trap corresponds to an effective magnetic field Ω_c pointing in some direction $\hat{\boldsymbol{d}}$ in the *yz* plane. The total effective magnetic field $\hat{\boldsymbol{\zeta}}\Omega_{\mathrm{tot}} = \hat{\boldsymbol{z}}\Omega + \hat{\boldsymbol{d}}\Omega_c$ is given by the vector sum of the intrinsic $\hat{\boldsymbol{z}}\Omega$ and applied $\hat{\boldsymbol{d}}\Omega_c$ fields. The effective spin precesses about the total magnetic field $\hat{\boldsymbol{\zeta}}\Omega_{\mathrm{tot}}$ which thus defines the quantization direction $\hat{\boldsymbol{\zeta}}$ and the two eigenstates $|\uparrow\rangle_\zeta$ and $|\downarrow\rangle_\zeta$ corresponding to the standing-wave (double-lobe) modes with orthogonal orientation. These two

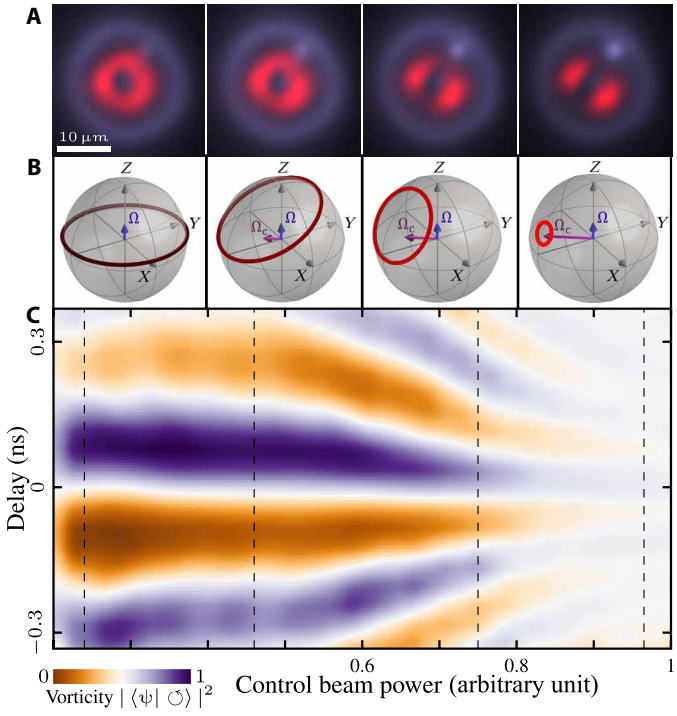

Fig. 4. Oscillation control and state initialization. (**A**) Polariton condensate photoluminescence (red) in a laser trap (light blue) for increasing intensity of the control beam (bright blue spot). A weak control beam contributes to the coupling between the two vortex states $|\circlearrowleft\rangle$ and $|\circlearrowright\rangle$, while a strong control beam pins the condensate to a standing-wave with a node at the beam position, i.e., the two lobes avoiding the beam. (**B**) Oscillation trajectories (one period) of the effective spin on the Bloch sphere with the original orientation of the axes for four different intensities of the control beam as in (A). The position and strength of the control beam define the direction and magnitude of the effective magnetic field Ω_c that adds to the intrinsic field Ω. (**C**) Condensate oscillation dynamics versus the control beam power. For a very weak beam, the oscillation period $\pi/\Omega \simeq 120$ ps between the two vortex states is determined by the effective magnetic field Ω due to the intrinsic disorder of the trapping potential. Stronger control beam leads to an increase of oscillation frequency Ω_{tot} and suppression of population of the higher energy eigenstate $|\downarrow\rangle_\zeta$ with one of the lobes on top of the potential energy bump induced by the beam, which decreased the oscillation amplitude.

eigenstates are split by $\mp\Omega_{tot}$, and the dynamics of the system is given by

$$|\psi(t)\rangle = c_0 e^{i\Omega_{tot}t}|\uparrow\rangle_\zeta + c_1 e^{-i\Omega_{tot}t}|\downarrow\rangle_\zeta \qquad (6)$$

where $|c_{0,1}|^2$ are the stationary populations of the two eigenstates. For equal populations $|c_0|^2 = |c_1|^2$, the effective spin processes in the plane perpendicular to $\hat{\boldsymbol{\zeta}}$ passing through the two vortex states $|\circlearrowleft\rangle = (|\uparrow\rangle_\zeta + |\downarrow\rangle_\zeta)/\sqrt{2}$ and $|\circlearrowright\rangle = (|\uparrow\rangle_\zeta - |\downarrow\rangle_\zeta)/\sqrt{2}$. But with increasing imbalance, $|c_0|^2 > |c_1|^2$, this oscillation amplitude is decreasing, and for $|c_0|^2 \gg |c_1|^2$, the effective spin is pinned to the lower energy state $|\uparrow_\zeta\rangle$.

In the polariton picture, the stronger control beam leading to reflection of the polariton current increases the energy separation between the two standing-wave eigenmodes. But the same localized potential barrier simultaneously increases the polariton scattering in all directions. This scattering, or extra loss, affects only the higher energy eigenmode with the antinode at the potential barrier, which induces imbalance of populations $|c_0|^2 \gg |c_1|^2$ (see Supplementary Materials S3).

Coherence measurements

The above experimental and theoretical analysis is relevant for times shorter than the coherence time τ_c of the system. We now use a Mach-Zehnder interferometer to perform measurements of the first-order correlation function of the polariton condensate

$$g^{(1)}(\boldsymbol{r},\tau) \propto \lim_{T\to\infty}\frac{1}{T}\int_0^T \psi(\boldsymbol{r},t)\ \psi^*(\boldsymbol{r},t+\tau)\ dt \qquad (7)$$

Selecting different positions $\boldsymbol{r}$ of the condensate, we can measure the correlation function for the individual polaritonic eigenmodes $\psi_{0,1}(\boldsymbol{r})$ and their superposition, as shown in Fig. 5 and detailed in Supplementary Materials S4. We then fit the experimentally measured coherences for the two eigenmodes with $|g_{0,1}^{(1)}(\tau)| \simeq e^{-(\tau/\tau_{c0,c1})^2}$ and for their superposition with $|g^{(1)}(\tau)| \simeq \frac{1}{2}\left[|g_0^{(1)}(\tau)|\cos(2\Omega\tau) + |g_1^{(1)}(\tau)|\right]$

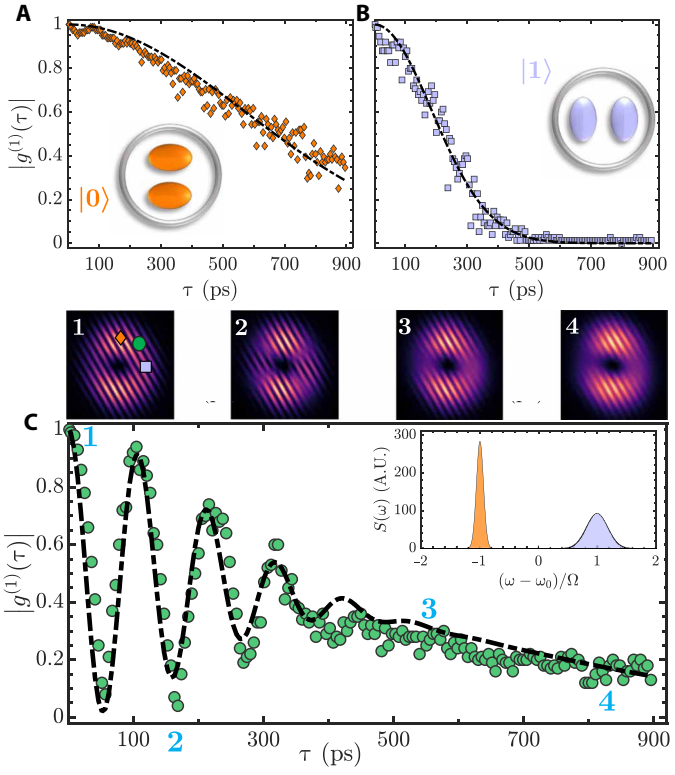

Fig. 5. Coherence measurements. Time dependence of the absolute value of the first-order correlation function $|g^{(1)}(\tau)|$ as obtained from the experimental measurements (filled circles) and fitted with the theoretical two-mode model (dashed lines) yielding the coherence times $\tau_{c0} \simeq 260$ ps and $\tau_{c1} \simeq 800$ ps. Correlation functions of the lower (**A**) and higher (**B**) energy states $|0\rangle$ and $|1\rangle$ and correlation function for the superposition of the two states (**C**). Panels (1, 2, 3, and 4) above (C) show the corresponding interferograms at time delays $\tau \simeq 0$,170,580, and 805 ps, while the filled symbols of different colors in (1) mark the positions of the interferometric measurements of $|g^{(1)}(\tau)|$ for graphs (A) to (C). The inset in (C) shows the power spectrum $S(\omega)$ of the polariton field (A.U., arbitrary units), as obtained from the Fourier transform of $g^{(1)}(\tau)$, illustrating the splitting of the eigenmodes by $\mp\Omega$ each having the width $\sqrt{2}/\tau_{c0}$ and $\sqrt{2}/\tau_{c1}$.

extracting thereby the corresponding coherence times and beating frequency 2Ω.

In the inset of Fig. 5C, we also show the power spectrum of the polariton field

$$S(\omega) \propto \tau_{c0} e^{-\left[(\omega+\Omega)\tau_{c0}/2\right]^2} + \tau_{c1} e^{-\left[(\omega-\Omega)\tau_{c1}/2\right]^2} \quad (8)$$

as obtained via the Fourier transform of the theoretical fit of $g^{(1)}$ (see Supplementary Materials S4). The spectrum consists of two Gaussians corresponding to the polariton eigemodes $\psi_{0,1}$ split by $\mp\Omega$ and having the widths $\sqrt{2}/\tau_{c0,c1}$.

Consistent with the previous studies (*58*), we observe that the polariton condensates spatially separated from the trapping potential can exhibit ultralong coherence times. Yet, we obtain that the polaritonic eigenmodes $\psi_0(\boldsymbol{r})$ and $\psi_1(\boldsymbol{r})$ have different coherence times $\tau_{c0} > \tau_{c1}$. We explain this difference by the proximity of the wave function of the corresponding eigenmode to the laser-induced trapping potential which is subject to the exciton number fluctuations and laser noise. The lower energy eigenmode having the two-lobe wave function $\psi_0(\boldsymbol{r})$ well separated from the walls of the confining potential has longer coherence time than the higher energy eigenmode $\psi_1(\boldsymbol{r})$ whose two lobes have larger overlap with the confining potential and therefore susceptible to more dephasing.

DISCUSSION

To summarize, we have experimentally realized and characterized a hitherto unexplored semiconductor exciton-polariton condensate system that exhibits unique properties, including long coherence times and persistent oscillations between two energy-degenerate vortex states $|\circlearrowleft\rangle$, $|\circlearrowright\rangle$ with tunable frequency Ω. We may argue that our polaritonic system, being equivalent to a spin-$^1/_2$ in a magnetic field Ω, is a promising candidate for quantum information applications. The two eigenstates of the polaritonic condensate split by $\mp\Omega$ can serve as the qubit basis states $|0,1\rangle = (|\circlearrowleft\rangle \pm |\circlearrowright\rangle)/\sqrt{2}$ equivalent to the spin states $|\uparrow, \downarrow\rangle_z$. The coherent oscillations between the vortex states due to elastic scattering are equivalent to the spin precession in the *xy* plane perpendicular to the magnetic field direction along *z*. Using an auxiliary control laser beam, we can control the oscillation frequency and even initialize the qubit to the well-defined state, e.g., $|0\rangle$. Moreover, by changing the position of the sufficiently strong control beam, we can overwrite the asymmetry of the confining potential or the position of the intrinsic defect, which would amount to the rotation of the direction of the effective magnetic field in the *yz* plane. This will induce coherent qubit rotations in any plane containing the *x* axis of the Bloch sphere in Fig. 1. Last, by stroboscopic application of suitable control beams, we may implement spin-echo or bang-bang operations to freeze the state of the qubit when required. Complemented with the controllable interactions between pairs of polaritonic qubits (see Supplementary Materials S5), such systems can simulate a large subset of quantum computing algorithms that do not rely on entanglement or projective measurements of the genuine qubits (*44*–*48*).

Future work will require additional efforts to demonstrate higher degree of control and longer coherence times of the analog polaritonic qubits by optimizing the trapping potentials and to implement controlled interactions and gate operations between such qubits. Apart from potential applications in analog quantum computing and simulations, our work provides a versatile platform for generating and manipulating structured nonlinear light with controlled topological charge, leveraging the intrinsic ultrafast modulation speed of polaritonic condensate systems.

Supplementary Materials

This PDF file includes:

Supplementary Text
Figs. S1 to S4
References

REFERENCES AND NOTES

1. H. Deng, H. Haug, Y. Yamamoto, Exciton-polariton bose-einstein condensation. *Rev. Mod. Phys.* **82**, 1489–1537 (2010).
2. I. Carusotto, C. Ciuti, Quantum fluids of light. *Rev. Mod. Phys.* **85**, 299–366 (2013).
3. H. Deng, G. Weihs, C. Santori, J. Bloch, Y. Yamamoto, Condensation of semiconductor microcavity exciton polaritons. *Science* **298**, 199–202 (2002).
4. J. Kasprzak, M. Richard, S. Kundermann, A. Baas, P. Jeambrun, J. M. J. Keeling, F. M. Marchetti, M. H. Szymańska, R. André, J. L. Staehli, V. Savona, P. B. Littlewood, B. Deveaud, L. S. Dang, Bose-Einstein condensation of exciton polaritons. *Nature* **443**, 409–414 (2006).
5. A. Imamog, R. J. Ram, S. Pau, Y. Yamamoto, Nonequilibrium condensates and lasers without inversion: Exciton-polariton lasers. *Phys. Rev. A* **53**, 4250–4253 (1996).
6. S. Christopoulos, G. B. H. Von Högersthal, A. J. D. Grundy, P. G. Lagoudakis, A. V. Kavokin, J. J. Baumberg, G. Christmann, R. Butté, E. Feltin, J.-F. Carlin, N. Grandjean, Room-temperature polariton lasing in semiconductor microcavities. *Phys. Rev. Lett.* **98**, 126405 (2007).
7. D. Sanvitto, S. Kéna-Cohen, The road towards polaritonic devices. *Nat. Mater.* **15**, 1061–1073 (2016).
8. J. L. O'brien, A. Furusawa, J. Vučković, Photonic quantum technologies. *Nat. Photonics* **3**, 687–695 (2009).
9. D. M. Coles, N. Somaschi, P. Michetti, C. Clark, P. G. Lagoudakis, P. G. Savvidis, D. G. Lidzey, Polariton-mediated energy transfer between organic dyes in a strongly coupled optical microcavity. *Nat. Mater.* **13**, 712–719 (2014).
10. A. Amo, J. Bloch, Exciton-polaritons in lattices: A non-linear photonic simulator. *C. R. Phys.* **17**, 934–945 (2016).
11. N. Y. Kim, Y. Yamamoto, "Exciton-polariton quantum simulators" in *Quantum Simulations with Photons and Polaritons: Merging Quantum Optics with Condensed Matter Physics* (2017), pp. 91–121.
12. N. G. Berloff, M. Silva, K. Kalinin, A. Askitopoulos, J. D. Töpfer, P. Cilibrizzi, W. Langbein, P. G. Lagoudakis, Realizing the classical XY Hamiltonian in polariton simulators. *Nat. Mater.* **16**, 1120–1126 (2017).
13. Y. Xue, I. Chestnov, E. Sedov, E. Kiktenko, A. K. Fedorov, S. Schumacher, X. Ma, A. Kavokin, Split-ring polariton condensates as macroscopic two-level quantum systems. *Phys. Rev. Res.* **3**, 013099 (2021).
14. A. Kavokin, T. C. Liew, C. Schneider, P. G. Lagoudakis, S. Klembt, S. Hoefling, Polariton condensates for classical and quantum computing. *Nat. Rev. Phys.* **4**, 435–451 (2022).
15. J. E. Mooij, T. P. Orlando, L. Levitov, L. Tian, C. H. Van der Wal, S. Lloyd, Josephson persistent-current qubit. *Science* **285**, 1036–1039 (1999).
16. I. Chiorescu, Y. Nakamura, C. J. P. M. Harmans, J. E. Mooij, Coherent quantum dynamics of a superconducting flux qubit. *Science* **299**, 1869–1871 (2003).
17. J. Q. You, F. Nori, Atomic physics and quantum optics using superconducting circuits. *Nature* **474**, 589–597 (2011).
18. F. Arute, K. Arya, R. Babbush, D. Bacon, J. C. Bardin, R. Barends, R. Biswas, S. Boixo, F. G. S. L. Brandao, D. A. Buell, B. Burkett, Y. Chen, Z. Chen, B. Chiaro, R. Collins, W. Courtney, A. Dunsworth, E. Farhi, B. Foxen, A. Fowler, C. Gidney, M. Giustina, R. Graff, K. Guerin, S. Habegger, M. P. Harrigan, M. J. Hartmann, A. Ho, M. Hoffmann, T. Huang, T. S. Humble, S. V. Isakov, E. Jeffrey, Z. Jiang, D. Kafri, K. Kechedzhi, J. Kelly, P. V. Klimov, S. Knysh, A. Korotkov, F. Kostritsa, D. Landhuis, M. Lindmark, E. Lucero, D. Lyakh, S. Mandrà, J. R. Mc Clean, M. M. Ewen, A. Megrant, X. Mi, K. Michielsen, M. Mohseni, J. Mutus, O. Naaman, M. Neeley, C. Neill, M. Y. Niu, E. Ostby, A. Petukhov, J. C. Platt, C. Quintana, E. G. Rieffel, P. Roushan, N. C. Rubin, D. Sank, K. J. Satzinger, V. Smelyanskiy, K. J. Sung, M. D. Trevithick, A. Vainsencher, B. Villalonga, T. White, Z. J. Yao, P. Yeh, A. Zalcman, H. Neven, J. M. Martinis, Quantum supremacy using a programmable superconducting processor. *Nature* **574**, 505–510 (2019).
19. K. G. Lagoudakis, M. Wouters, M. Richard, A. Baas, I. Carusotto, R. André, L. S. Dang, B. Deveaud-Plédran, Quantized vortices in an exciton-polariton condensate. *Nat. Phys.* **4**, 706–710 (2008).

20. K. G. Lagoudakis, T. Ostatnická, A. V. Kavokin, Y. G. Rubo, R. André, B. Deveaud-Plédran, Observation of half-quantum vortices in an exciton-polariton condensate. *Science* **326**, 974–976 (2009).
21. F. Manni, K. G. Lagoudakis, T. C. H. Liew, R. André, V. Savona, B. Deveaud, Dissociation dynamics of singly charged vortices into half-quantum vortex pairs. *Nat. Commun.* **3**, 1309 (2012).
22. G. Grosso, G. Nardin, F. Morier-Genoud, Y. Léger, B. Deveaud-Plédran, Soliton instabilities and vortex street formation in a polariton quantum fluid. *Phys. Rev. Lett.* **107**, 245301 (2011).
23. G. Nardin, G. Grosso, Y. Leger, B. Pietka, F. Morier-Genoud, B. Deveaud-Pledran, Hydrodynamic nucleation of quantized vortex pairs in a polariton quantum fluid. *Nat. Phys.* **7**, 635–641 (2011).
24. R. Dall, M. D. Fraser, A. S. Desyatnikov, G. Li, S. Brodbeck, M. Kamp, C. Schneider, S. Höfling, E. A. Ostrovskaya, Creation of orbital angular momentum states with chiral polaritonic lenses. *Phys. Rev. Lett.* **113**, 200404 (2014).
25. T. Gao, G. Li, E. Estrecho, T. C. H. Liew, D. Comber-Todd, A. Nalitov, M. Steger, K. West, L. Pfeiffer, D. W. Snoke, A. V. Kavokin, A. G. Truscott, E. A. Ostrovskaya, Chiral modes at exceptional points in exciton-polariton quantum fluids. *Phys. Rev. Lett.* **120**, 065301 (2018).
26. T. Gao, O. A. Egorov, E. Estrecho, K. Winkler, M. Kamp, C. Schneider, S. Höfling, A. G. Truscott, E. A. Ostrovskaya, Controlled ordering of topological charges in an exciton-polariton chain. *Phys. Rev. Lett.* **121**, 225302 (2018).
27. E. S. Sedov, V. A. Lukoshkin, V. K. Kalevich, P. G. Savvidis, A. V. Kavokin, Circular polariton currents with integer and fractional orbital angular momenta. *Phys. Rev. Res.* **3**, 013072 (2021).
28. E. Aladinskaia, R. Cherbunin, E. Sedov, A. Liubomirov, K. Kavokin, E. Khramtsov, M. Petrov, P. G. Savvidis, A. Kavokin, Spatial quantization of exciton-polariton condensates in optically induced traps. *Phys. Rev. B* **107**, 045302 (2023).
29. V. A. Lukoshkin, V. K. Kalevich, M. M. Afanasiev, K. V. Kavokin, Z. Hatzopoulos, P. G. Savvidis, E. S. Sedov, A. V. Kavokin, Persistent circular currents of exciton-polaritons in cylindrical pillar microcavities. *Phys. Rev. B* **97**, 195149 (2018).
30. B. Real, N. Carlon Zambon, P. St-Jean, I. Sagnes, A. Lemaître, L. Le Gratiet, A. Harouri, S. Ravets, J. Bloch, A. Amo, Chiral emission induced by optical Zeeman effect in polariton micropillars. *Phys. Rev. Res.* **3**, 043161 (2021).
31. D. Sanvitto, F. M. Marchetti, M. H. Szymańska, G. Tosi, M. Baudisch, F. P. Laussy, D. N. Krizhanovskii, M. S. Skolnick, L. Marrucci, A. Lemaître, J. Bloch, C. Tejedor, L. Viña, Persistent currents and quantized vortices in a polariton superfluid. *Nat. Phys.* **6**, 527–533 (2010).
32. M. S. Kwon, B. Y. Oh, S. H. Gong, J. H. Kim, H. K. Kang, S. Kang, J. D. Song, H. Choi, Y. H. Cho, Direct transfer of light's orbital angular momentum onto a nonresonantly excited polariton superfluid. *Phys. Rev. Lett.* **122**, 045302 (2019).
33. L. Dominici, N. Voronova, D. Colas, A. Gianfrate, A. Rahmani, V. Ardizzone, D. Ballarini, M. De Giorgi, G. Gigli, F. P. Laussy, D. Sanvitto, Shaping the topology of light with a moving Rabi-oscillating vortex. *Opt. Express* **29**, 37262–37280 (2021).
34. D. Choi, M. Park, B. Y. Oh, M. S. Kwon, S. I. Park, S. Kang, J. D. Song, D. Ko, M. Sun, I. G. Savenko, Y. H. Cho, H. Choi, Observation of a single quantized vortex vanishment in exciton-polariton superfluids. *Phys. Rev. B* **105**, L060502 (2022).
35. X. Ma, B. Berger, M. Aßmann, R. Driben, T. Meier, C. Schneider, S. Höfling, S. Schumacher, Realization of all-optical vortex switching in exciton-polariton condensates. *Nat. Commun.* **11**, 897 (2020).
36. S. Alyatkin, C. Milian, Y. V. Kartashov, K. A. Sitnik, J. D. Topfer, H. Sigurdsson, P. G. Lagoudakis, All-optical artificial vortex matter in quantum fluids of light. *Sci. Adv.* **10**, eadj1589 (2024).
37. K. A. Sitnik, S. Alyatkin, J. D. Töpfer, I. Gnusov, T. Cookson, H. Sigurdsson, P. G. Lagoudakis, Spontaneous formation of time-periodic vortex cluster in nonlinear fluids of light. *Phys. Rev. Lett.* **128**, 237402 (2022).
38. K. A. Sitnik, I. Gnusov, M. Misko, J. D. Töpfer, S. Alyatkin, P. G. Lagoudakis, Control of the oscillation frequency of a vortex cluster in the trapped polariton condensate. *Appl. Phys. Lett.* **124**, 201102 (2024).
39. F. Manni, K. G. Lagoudakis, T. C. H. Liew, R. André, B. Deveaud-Plédran, Spontaneous pattern formation in a polariton condensate. *Phys. Rev. Lett.* **107**, 106401 (2011).
40. A. Dreismann, P. Cristofolini, R. Balili, G. Christmann, F. Pinsker, N. G. Berloff, Z. Hatzopoulos, P. G. Savvidis, J. J. Baumberg, Coupled counterrotating polariton condensates in optically defined annular potentials. *Proc. Natl. Acad. Sci. U.S.A.* **111**, 8770–8775 (2014).
41. J. Wang, H. Xu, R. Su, Y. Peng, J. Wu, T. C. H. Liew, Q. Xiong, Spontaneously coherent orbital coupling of counterrotating exciton polaritons in annular perovskite microcavities. *Light Sci. Appl.* **10**, 45 (2021).
42. S. Zhang, Z. Zhu, W. Du, X. Wu, S. Ghosh, Q. Zhang, Q. Xiong, X. Liu, All-optical control of rotational exciton polaritons condensate in perovskite microcavities. *ACS Photonics* **10**, 2414–2422 (2023).
43. I. Gnusov, S. Harrison, S. Alyatkin, K. Sitnik, J. Töpfer, H. Sigurdsson, P. G. Lagoudakis, Quantum vortex formation in the "rotating bucket" experiment with polariton condensates. *Sci. Adv.* **9**, eadd1299 (2023).
44. T. Byrnes, K. Wen, Y. Yamamoto, Macroscopic quantum computation using Bose-Einstein condensates. *Phys. Rev. A* **85**, 040306 (2012).
45. E. Biham, G. Brassard, D. Kenigsberg, T. Mor, Quantum computing without entanglement. *Theor. Comput. Sci.* **320**, 15–33 (2004).
46. B. P. Lanyon, M. Barbieri, M. P. Almeida, A. G. White, Experimental quantum computing without entanglement. *Phys. Rev. Lett.* **101**, 200501 (2008).
47. M. Balynsky, H. Chiang, D. Gutierrez, A. Kozhevnikov, Y. Filimonov, A. Khitun, Quantum computing without quantum computers: Database search and data processing using classical wave superposition. *J. Appl. Phys.* **130**, 164903 (2021).
48. M. Mohseni, V. I. Vasyuchka, V. S. L'vov, A. A. Serga, B. Hillebrands, Classical analog of qubit logic based on a magnon Bose-Einstein condensate. *Commun. Phys.* **5**, 196 (2022).
49. S. V. Mukherjee, K. Kozin, A. V. Nalitov, I. A. Shelykh, Z. Sun, D. M. Myers, B. Ozden, J. Beaumariage, M. Steger, L. N. Pfeiffer, K. West, D. W. Snoke, Dynamics of spin polarization in tilted polariton rings. *Phys. Rev. B* **103**, 165306 (2021).
50. G. Liu, D. W. Snoke, A. Daley, L. N. Pfeiffer, K. West, A new type of half-quantum circulation in a macroscopic polariton spinor ring condensate. *Proc. Natl. Acad. Sci. U.S.A.* **112**, 2676–2681 (2015).
51. L. Dominici, G. Dagvadorj, J. M. Fellows, D. Ballarini, M. De Giorgi, F. M. Marchetti, B. Piccirillo, L. Marrucci, A. Bramati, G. Gigli, M. H. Szymańska, D. Sanvitto, Vortex and half-vortex dynamics in a nonlinear spinor quantum fluid. *Sci. Adv.* **1**, e1500807 (2015).
52. I. Gnusov, H. Sigurdsson, J. D. Töpfer, S. Baryshev, S. Alyatkin, P. G. Lagoudakis, All-optical linear-polarization engineering in single and coupled exciton-polariton condensates. *Phys. Rev. Appl.* **16**, 034014 (2021).
53. M. Pukrop, S. Schumacher, X. Ma, Circular polarization reversal of half-vortex cores in polariton condensates. *Phys. Rev. B* **101**, 205301 (2020).
54. S. Demirchyan, I. Chestnov, K. Kondratenko, A. K. Kavokin, Spinor superfluid currents of exciton-polaritons on a split-ring. arXiv:2208.14094 [cond-mat.mes-hall] (2022).
55. D. Aristov, H. Sigurdsson, P. G. Lagoudakis, Screening nearest-neighbor interactions in networks of exciton-polariton condensates through spin-orbit coupling. *Phys. Rev. B* **105**, 155306 (2022).
56. I. Gnusov, H. Sigurdsson, S. Baryshev, T. Ermatov, A. Askitopoulos, P. G. Lagoudakis, Optical orientation, polarization pinning, and depolarization dynamics in optically confined polariton condensates. *Phys. Rev. B* **102**, 125419 (2020).
57. H. Sigurdsson, I. Gnusov, S. Alyatkin, L. Pickup, N. A. Gippius, P. G. Lagoudakis, A. Askitopoulos, Persistent self-induced larmor precession evidenced through periodic revivals of coherence. *Phys. Rev. Lett.* **129**, 155301 (2022).
58. K. Orfanakis, A. F. Tzortzakakis, D. Petrosyan, P. G. Savvidis, H. Ohadi, Ultralong temporal coherence in optically trapped exciton-polariton condensates. *Phys. Rev. B* **103**, 235313 (2021).
59. P. Tsotsis, P. S. Eldridge, T. Gao, S. I. Tsintzos, Z. Hatzopoulos, P. G. Savvidis, Lasing threshold doubling at the crossover from strong to weak coupling regime in GaAs microcavity. *New J. Phys.* **14**, 023060 (2012).
60. S. Kim, B. Zhang, Z. Wang, J. Fischer, S. Brodbeck, M. Kamp, C. Schneider, S. Höfling, H. Deng, Coherent polariton laser. *Phys. Rev. X* **6**, 011026 (2016).
61. P. Lambropoulos, D. Petrosyan, *Fundamentals of Quantum Optics and Quantum Information* (Springer, 2007).
62. M. A. Nielsen, I. L. Chuang, *Quantum Computation and Quantum Information* (Cambridge Univ. Press, 2000).

Acknowledgments

Funding: J.B., M.N., X.Z., G.G.P., and P.G.S. acknowledge the support of Innovation Program for Quantum Science and Technology (2023ZD0300300), Westlake University project no. 041020100118, and Zhejiang Provincial Natural Science Foundation (XHD24A2401). P.G.S. acknowledges financial support from the Horizon EIC-2022-Pathfinderchallenges-01 Heisenberg project 101114978. A.F.T. and D.P. were supported by the EU QuantERA Project PACE-IN (GSRT grant no. T11EPA4-00015) and HORIZON-RIA Project EuRyQa (grant no. 101070144). **Author contributions:** J.B., G.G.P., X.Z., and P.G.S. designed the experiment. J.B. and M.N. performed the experiments and analyzed the data. J.B. developed the software for the data acquisition. A.F.T. and D.P. developed the theory and carried out numerical simulations. P.G.S. supervised the project. All the authors participated in the writing and revision of the manuscript. **Competing interests:** The authors declare that they have no competing interests. **Data and materials availability:** All data needed to evaluate the conclusions in the paper are present in the paper and/or the Supplementary Materials.

Submitted 31 January 2024
Accepted 17 September 2024
Published 23 October 2024
10.1126/sciadv.ado4042